Energetics of the sperm flagellum

David J. Smith,
Hermes Gadêlha, Eamonn Gaffney, John Blake
and Jackson Kirkman-Brown

School of Mathematics
University of Birmingham

MOTIMO Final Meeting,
22nd September 2015

Outline

The female reproductive tract

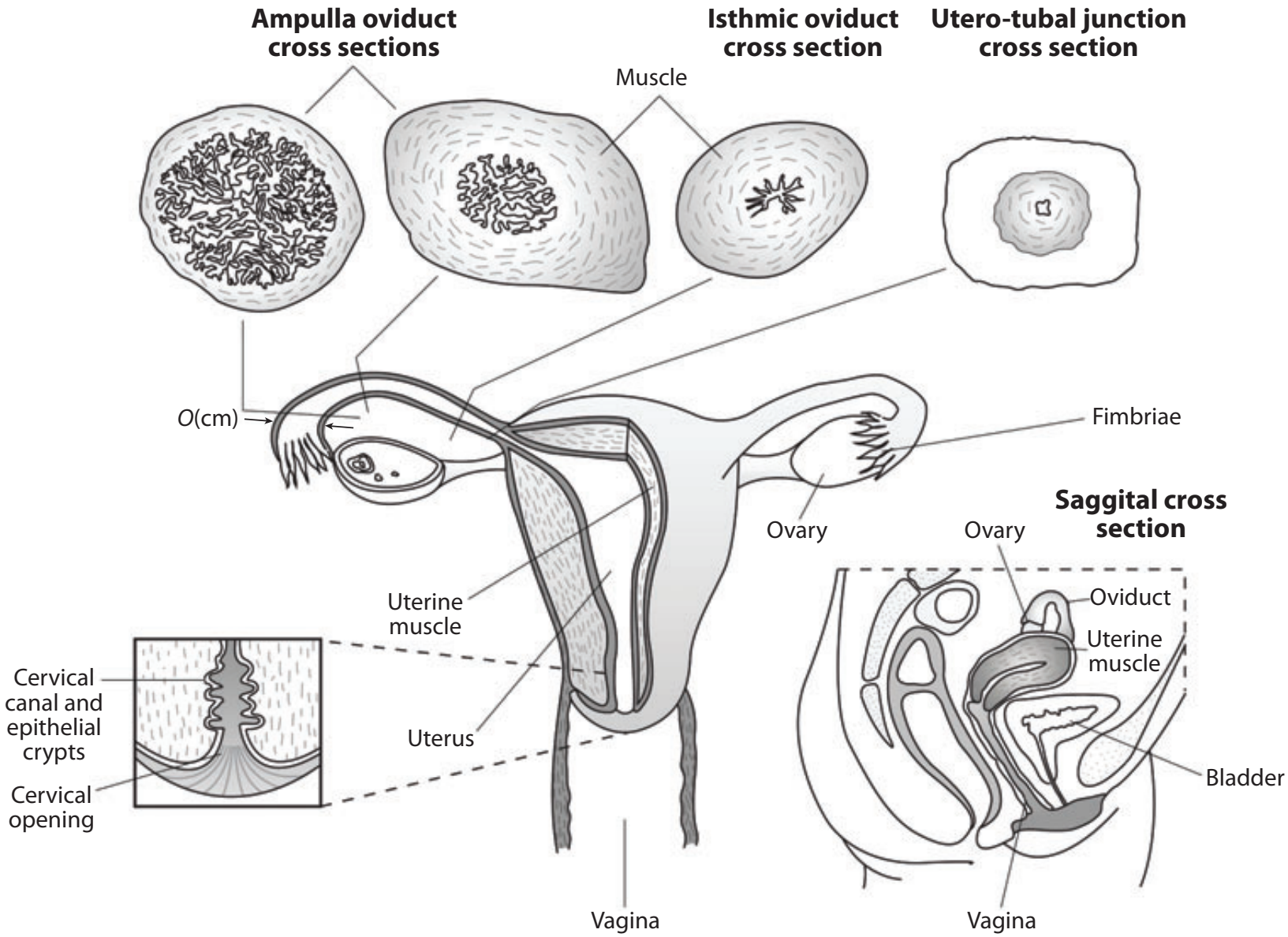

Sperm migration

- In natural fertilisation, an initial population of several hundred million sperm is reduced to tens or hundreds near the egg, and at most one fertilising cell.

Sperm migration

- In natural fertilisation, an initial population of several hundred million sperm is reduced to tens or hundreds near the egg, and at most one fertilising cell.
- Sperm actively migrate several thousand body lengths by beating their flagella.

Sperm migration

- In natural fertilisation, an initial population of several hundred million sperm is reduced to tens or hundreds near the egg, and at most one fertilising cell.
- Sperm actively migrate several thousand body lengths by beating their flagella.
- This migration is through viscous and/or viscoelastic fluid, including mucus and the cumulus mass surrounding the egg.

The human sperm

- Human sperm swim at up to about 100 μm/s; the tail beat frequency is anywhere from 2-30 Hz depending on temperature, liquid properties and biochemistry.

The human sperm

- Human sperm swim at up to about 100 μm/s; the tail beat frequency is anywhere from 2-30 Hz depending on temperature, liquid properties and biochemistry.
- A typical 'physiological' migratory cell will beat at 10-15 Hz and swim at 50 μm/s in cervical mucus substitute.

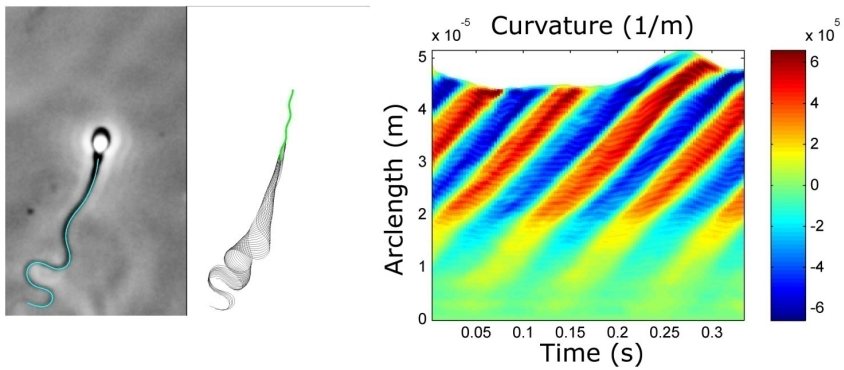

Figure 3. Imaging and analysis of a sperm cell in high viscosity

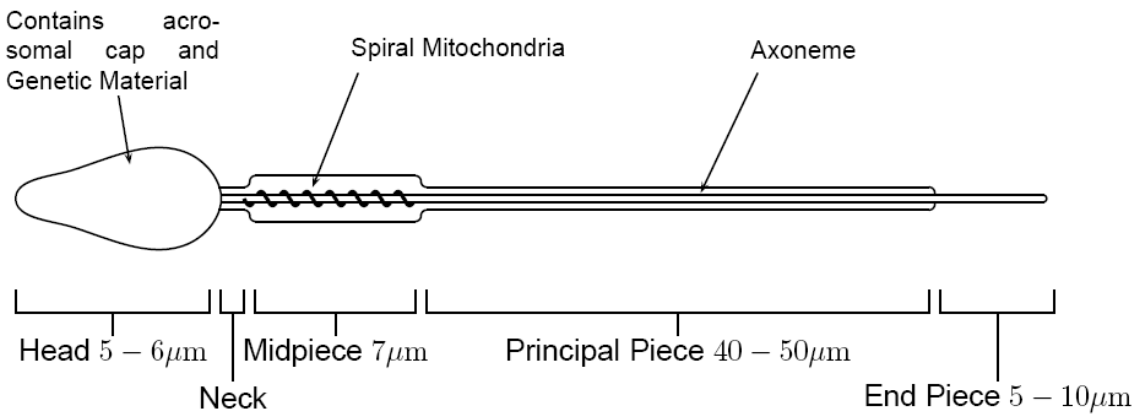

Different strokes

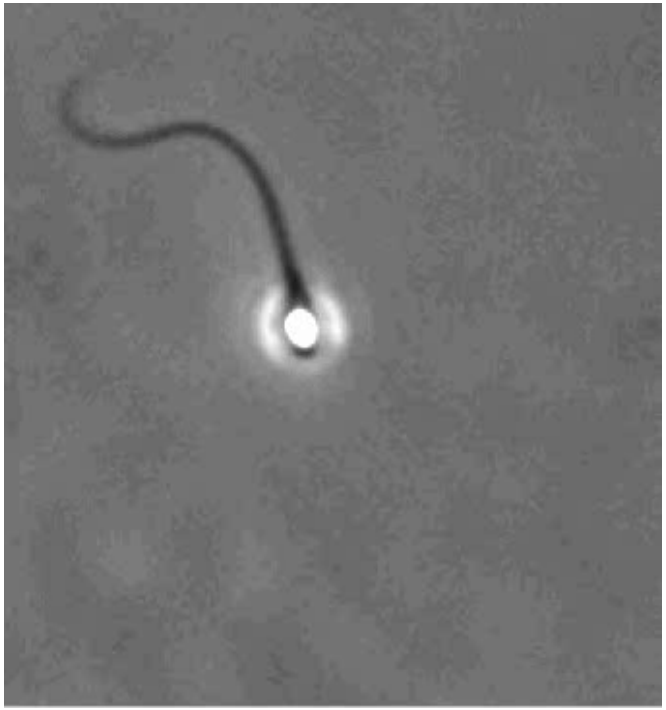

Low viscosity sperm

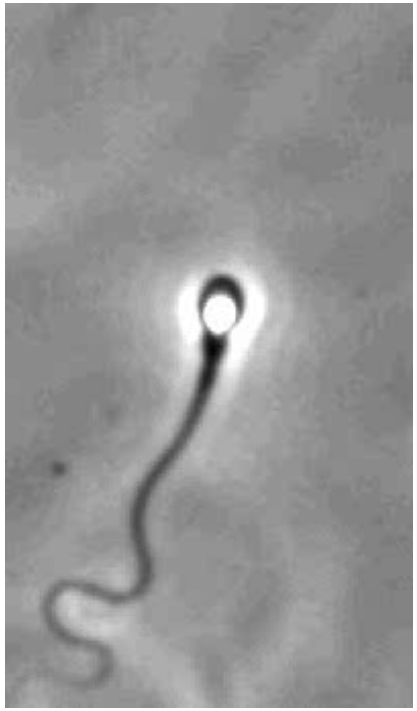

High viscosity sperm

The importance of sperm energy metabolism

Perhaps due to Purcell's famous 1976 lecture... is energy a limiting factor in microscale propulsion?

The importance of sperm energy metabolism

Perhaps due to Purcell's famous 1976 lecture... is energy a limiting factor in microscale propulsion? There is significant evidence of its importance in mammalian fertilisation, and considerable interest in the sperm biology community.

The importance of sperm energy metabolism

Perhaps due to Purcell's famous 1976 lecture... is energy a limiting factor in microscale propulsion? There is significant evidence of its importance in mammalian fertilisation, and considerable interest in the sperm biology community.

- There is a statistically significant correlation between infertility and mitochondrial volume in human sperm [Mundy et al. Hum. Reprod. 10:116-9, 1995].

The importance of sperm energy metabolism

Perhaps due to Purcell's famous 1976 lecture... is energy a limiting factor in microscale propulsion? There is significant evidence of its importance in mammalian fertilisation, and considerable interest in the sperm biology community.

- There is a statistically significant correlation between infertility and mitochondrial volume in human sperm [Mundy et al. Hum. Reprod. 10:116-9, 1995].
- Mitochondria occupy about 2×10^{-18} m^3 and can normally produce about 10^6 W/m^{-3} chemical power via ATP:ADP ratio, i.e. about 2×10^{-12} W.

The importance of sperm energy metabolism

Perhaps due to Purcell's famous 1976 lecture... is energy a limiting factor in microscale propulsion? There is significant evidence of its importance in mammalian fertilisation, and considerable interest in the sperm biology community.

- There is a statistically significant correlation between infertility and mitochondrial volume in human sperm [Mundy et al. Hum. Reprod. 10:116-9, 1995].
- Mitochondria occupy about 2×10^{-18} m^3 and can normally produce about 10^6 W/m^{-3} chemical power via ATP:ADP ratio, i.e. about 2×10^{-12} W.
- A fibre 5×10^{-5} m in length undergoing oscillations of 5×10^{-6} m at frequency 10 Hz in fluid of viscosity 0.2 Pa.s will cause viscous power dissipation of the order of 10^{-12} W.

The importance of sperm energy metabolism

Perhaps due to Purcell's famous 1976 lecture... is energy a limiting factor in microscale propulsion? There is significant evidence of its importance in mammalian fertilisation, and considerable interest in the sperm biology community.

- There is a statistically significant correlation between infertility and mitochondrial volume in human sperm [Mundy et al. Hum. Reprod. 10:116-9, 1995].
- Mitochondria occupy about 2×10^{-18} m^3 and can normally produce about 10^6 W/m^{-3} chemical power via ATP:ADP ratio, i.e. about 2×10^{-12} W.
- A fibre 5×10^{-5} m in length undergoing oscillations of 5×10^{-6} m at frequency 10 Hz in fluid of viscosity 0.2 Pa.s will cause viscous power dissipation of the order of 10^{-12} W.
- Energy *transport* is also important (enzymatic shuttles, local glycolysis, see reviews by C. Ford [Hum. Reprod. Update 12:269, 2006], also B. Storey, K. Miki, recent data in mouse by Takei et al. [J. Exp. Biol. 217:1876, 2014]).

Outline

Dynamics of incompressible fluid

Momentum and mass balance yield,

$$\rho\left(\frac{\partial \mathbf{u}^*}{\partial t^*} + (\mathbf{u}^* \cdot \nabla^*)\mathbf{u}^*\right) = \nabla^* \cdot \boldsymbol{\sigma}^*,$$

$$\nabla^* \cdot \mathbf{u}^* = 0,$$

where $\boldsymbol{\sigma}^*$ is the stress tensor, which can be divided into an isotropic part and a deviatoric part, $\sigma_{jk} = -p\delta_{jk} + \tau_{jk}$.

Dynamics of incompressible fluid

Momentum and mass balance yield,

$$\rho\left(\frac{\partial \mathbf{u}^*}{\partial t^*} + (\mathbf{u}^* \cdot \nabla^*)\mathbf{u}^*\right) = \nabla^* \cdot \boldsymbol{\sigma}^*,$$

$$\nabla^* \cdot \mathbf{u}^* = 0,$$

where $\boldsymbol{\sigma}^*$ is the stress tensor, which can be divided into an isotropic part and a deviatoric part, $\sigma_{jk} = -p\delta_{jk} + \tau_{jk}$.
A Newtonian fluid is defined by the constitutive law,

$$\tau_{jk} = \mu(\partial_j u_k + \partial_k u_j).$$

Very low Reynolds number flow

Newtonian incompressible flow is then described by the Navier-Stokes equations,

$$\rho\left(\frac{\partial \mathbf{u}^*}{\partial t^*} + (\mathbf{u}^* \cdot \nabla^*)\mathbf{u}^*\right) = -\boldsymbol{\nabla}^* p^* + \mu \nabla^{*2}\mathbf{u}^*,$$

$$\nabla^* \cdot \mathbf{u}^* = 0.$$

Very low Reynolds number flow

Newtonian incompressible flow is then described by the Navier-Stokes equations,

$$\rho\left(\frac{\partial \mathbf{u}^*}{\partial t^*} + (\mathbf{u}^* \cdot \nabla^*)\mathbf{u}^*\right) = -\boldsymbol{\nabla}^* p^* + \mu \nabla^{*2}\mathbf{u}^*,$$

$$\nabla^* \cdot \mathbf{u}^* = 0.$$

Nondimensionalising with respect to typical velocity scale U and length scale L yields the dimensionless equations,

$$\mathrm{Re}\left(\frac{\partial \mathbf{u}}{\partial t} + (\mathbf{u} \cdot \nabla)\mathbf{u}\right) = -\boldsymbol{\nabla} p + \mu \nabla^2 \mathbf{u}, \tag{1}$$

$$\nabla \cdot \mathbf{u} = 0, \tag{2}$$

where $\mathrm{Re} = \rho UL/\mu$ is the Reynolds number. Typical scales are $U = 50$ μm/s and $L = 50$ μm, so $\mathrm{Re} \ll 1$.

Stokes flow

- Very low Reynolds number physically means that inertia is negligible relative to viscosity.

$$0 = -\boldsymbol{\nabla} p + \mu \nabla^2 \mathbf{u}, \quad \boldsymbol{\nabla} \cdot \mathbf{u} = 0,$$

- This balance yields the 'Scallop Theorem' of E.M. Purcell (but known much earlier): a time-irreversible motion is essential for a cell to propel itself.

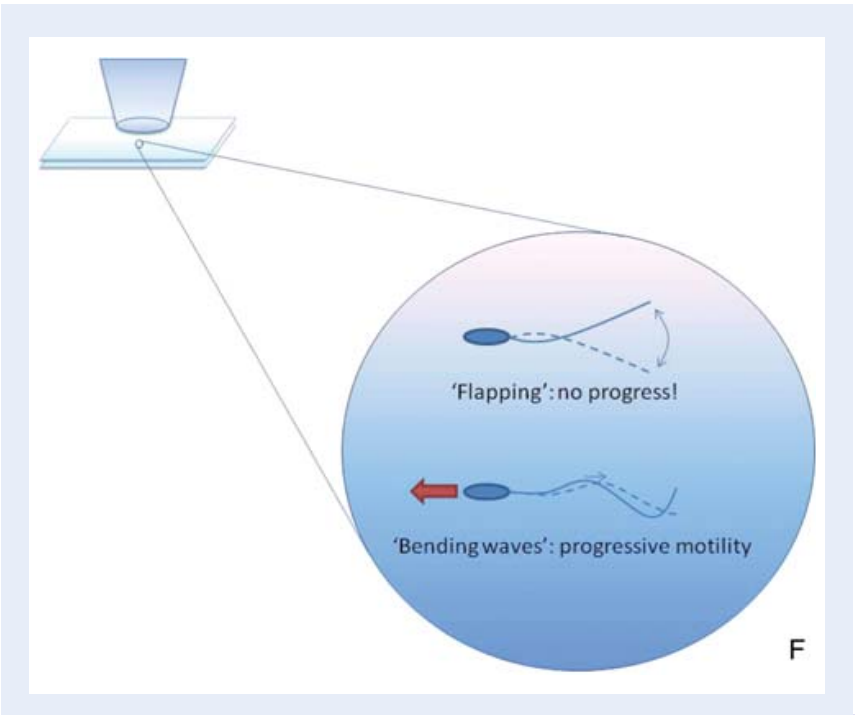

Irreversible beat pattern

- How is irreversibility achieved? Oblique movements cause a thrust in one direction through slender body drag anisotropy: $f_n \approx C_n u_n$, $f_t \approx C_t u_t$, $(C_n/C_t \approx 2)$.

Irreversible beat pattern

- How is irreversibility achieved? Oblique movements cause a thrust in one direction through slender body drag anisotropy: $f_n \approx C_n u_n$, $f_t \approx C_t u_t$, $(C_n/C_t \approx 2)$.
- Sperm swim by propagating waves; these waves cause oblique movements of the slender flagellum, the anisotropic drag law results in thrust (balanced by the drag on the head).

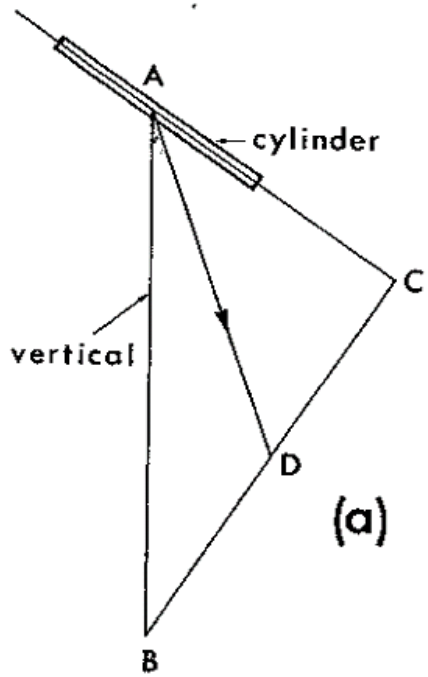

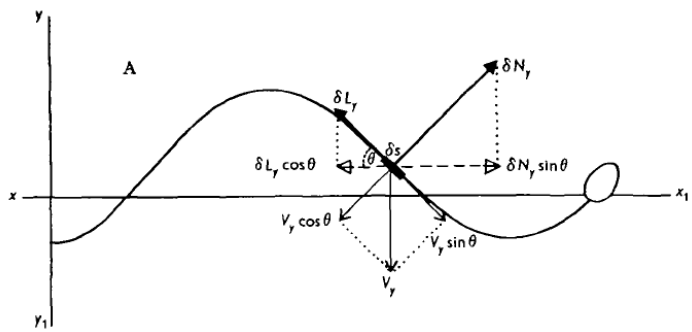

Boundary conditions

Biological flow problems typically involve moving, curved boundaries, e.g. the cell body, flagellum, cilia...

Boundary conditions

Biological flow problems typically involve moving, curved boundaries, e.g. the cell body, flagellum, cilia...
The fluid velocity at a material surface point $\mathbf{X}$ must satisfy the no-slip, no-penetration condition $\mathbf{u}(\mathbf{X}) = \partial_t \mathbf{X}$.

Boundary conditions

Biological flow problems typically involve moving, curved boundaries, e.g. the cell body, flagellum, cilia...
The fluid velocity at a material surface point $\mathbf{X}$ must satisfy the no-slip, no-penetration condition $\mathbf{u}(\mathbf{X}) = \partial_t \mathbf{X}$.
For the purpose of this talk, we will consider 'local' models only: assume that the flow around the cell approaches zero at long distances.

Boundary conditions

Biological flow problems typically involve moving, curved boundaries, e.g. the cell body, flagellum, cilia...
The fluid velocity at a material surface point $\mathbf{X}$ must satisfy the no-slip, no-penetration condition $\mathbf{u}(\mathbf{X}) = \partial_t \mathbf{X}$.
For the purpose of this talk, we will consider 'local' models only: assume that the flow around the cell approaches zero at long distances.
In many situations, boundaries are very important, e.g. epithelial surfaces, microscope slide... these surfaces can be dealt with via boundary integral methods and/or the method of images (e.g. the 'blakelet').

Mathematical approaches to flagellar propulsion

Linearity of the Stokes flow equations motivates methods based on superposition of fundamental solutions.

Mathematical approaches to flagellar propulsion

Linearity of the Stokes flow equations motivates methods based on superposition of fundamental solutions. The Stokes flow equations with spatially concentrated force are,

$$-\boldsymbol{\nabla} p + \nabla^2 u + \mathbf{e}_k \delta(\mathbf{x}) = 0, \tag{3}$$

$$\nabla \cdot \mathbf{u} = 0. \tag{4}$$

Mathematical approaches to flagellar propulsion

Linearity of the Stokes flow equations motivates methods based on superposition of fundamental solutions. The Stokes flow equations with spatially concentrated force are,

$$-\boldsymbol{\nabla} p + \nabla^2 u + \mathbf{e}_k \delta(\mathbf{x}) = 0, \tag{3}$$

$$\nabla \cdot \mathbf{u} = 0. \tag{4}$$

The velocity part of the solution defines the 'stokeslet'/Oseen tensor $S_{jk} := u_j$.

$$u_j(\mathbf{x}) = \frac{1}{8\pi}\left(\frac{\delta_{jk}}{r} + \frac{x_j x_k}{r^3}\right) =: S_{jk}(\mathbf{x}), \tag{5}$$

where $r = |\mathbf{x}|$.

Mathematical approaches to flagellar propulsion

Linearity of the Stokes flow equations motivates methods based on superposition of fundamental solutions. The Stokes flow equations with spatially concentrated force are,

$$-\boldsymbol{\nabla} p + \nabla^2 u + \mathbf{e}_k \delta(\mathbf{x}) = 0, \tag{3}$$

$$\nabla \cdot \mathbf{u} = 0. \tag{4}$$

The velocity part of the solution defines the 'stokeslet'/Oseen tensor $S_{jk} := u_j$.

$$u_j(\mathbf{x}) = \frac{1}{8\pi}\left(\frac{\delta_{jk}}{r} + \frac{x_j x_k}{r^3}\right) =: S_{jk}(\mathbf{x}), \tag{5}$$

where $r = |\mathbf{x}|$.
The pressure part yields,

$$p(\mathbf{x}) = \frac{1}{4\pi}\frac{x_k}{r^3} := P_k(\mathbf{x}).$$

Higher-order singularities

Spatial derivatives of stokeslets are also solutions of the Stokes flow equations:

Higher-order singularities

Spatial derivatives of stokeslets are also solutions of the Stokes flow equations:

Third-rank tensor (stokes doublet):

$$-\partial_\ell S_{jk} = \frac{1}{8\pi}\left(\frac{\delta_{jk}x_\ell}{r^3} - \frac{\delta_{j\ell}x_k}{r^3} - \frac{x_j\delta_{\ell k}}{r^3} + 3\frac{x_j x_k x_\ell}{r^5}\right).$$

This can be decomposed into an antisymmetric part (rotlet) and a symmetric part (stresslet).

Higher-order singularities

Spatial derivatives of stokeslets are also solutions of the Stokes flow equations:
Third-rank tensor (stokes doublet):

$$-\partial_\ell S_{jk} = \frac{1}{8\pi}\left(\frac{\delta_{jk}x_\ell}{r^3} - \frac{\delta_{j\ell}x_k}{r^3} - \frac{x_j\delta_{\ell k}}{r^3} + 3\frac{x_j x_k x_\ell}{r^5}\right).$$

This can be decomposed into an antisymmetric part (rotlet) and a symmetric part (stresslet).
Stresslets can be added to yield a source:

$$W_j := \delta_{\ell k}(-\partial_\ell S_{jk}) = \frac{1}{4\pi}\left(\frac{x_j}{r^3}\right),$$

Higher-order singularities

Spatial derivatives of stokeslets are also solutions of the Stokes flow equations:
Third-rank tensor (stokes doublet):

$$-\partial_\ell S_{jk} = \frac{1}{8\pi}\left(\frac{\delta_{jk}x_\ell}{r^3} - \frac{\delta_{j\ell}x_k}{r^3} - \frac{x_j\delta_{\ell k}}{r^3} + 3\frac{x_j x_k x_\ell}{r^5}\right).$$

This can be decomposed into an antisymmetric part (rotlet) and a symmetric part (stresslet).
Stresslets can be added to yield a source:

$$W_j := \delta_{\ell k}(-\partial_\ell S_{jk}) = \frac{1}{4\pi}\left(\frac{x_j}{r^3}\right),$$

differentiating further yields a source dipole (as in potential theory):

$$K_{jk} := -\partial_k W_j = \frac{1}{4\pi}\left(-\frac{\delta_{jk}}{r^3} + 3\frac{x_j x_k}{r^5}\right).$$

Stokes' Law

Stokeslets, rotlets, stresslets, source dipoles etc. can be used to construct solutions to flow problems. For example, the flow due to a sphere of radius a moving in with velocity $(0, 0, U)$ is given by,

$$u_j = 6\pi a U \delta_{k3} \left(\frac{1}{8\pi} \left(\frac{\delta_{jk}}{r} + \frac{x_j x_k}{r^3} \right) - \frac{a^2}{6} \frac{1}{4\pi} \left(-\frac{\delta_{jk}}{r^3} + 3\frac{x_j x_k}{r^5} \right) \right),$$

which satisfies $u_j = \delta_{j3} U$ on $r = a$, and yields Stokes' law that the (dimensional) drag on a sphere has magnitude $6\pi\mu a U$. The moment on a rotating sphere can be derived similarly via the rotlet.

Linear superposition of stokeslets

A concentrated point force located at $\mathbf{y}$ with strength $\mathbf{F}$, produces a velocity field (the 'stokeslet'/Oseen tensor),

$$u_j(\mathbf{x}) = S_{jk}(\mathbf{x} - \mathbf{y})F_k,$$

with the summation convention.

Linear superposition of stokeslets

A concentrated point force located at $\mathbf{y}$ with strength $\mathbf{F}$, produces a velocity field (the 'stokeslet'/Oseen tensor),

$$u_j(\mathbf{x}) = S_{jk}(\mathbf{x} - \mathbf{y})F_k,$$

with the summation convention.
Flow due to a slender body with centreline $\mathbf{X}(s)$ can be expressed approximately as,

$$u_j(\mathbf{x}) = \int_0^L S_{jk}(\mathbf{x}, \mathbf{X}(s'))f_k(s')ds',$$

where the force per unit length $f_k(s')$ is determined so that $u_j(\mathbf{X}(s) + a\mathbf{n}(s)) \approx \partial_t \mathbf{X}(s)$ where $\mathbf{n}(s)$ is a vector normal to the centreline and a is slender body radius (small).

Linear superposition of stokeslets

A concentrated point force located at $\mathbf{y}$ with strength $\mathbf{F}$, produces a velocity field (the 'stokeslet'/Oseen tensor),

$$u_j(\mathbf{x}) = S_{jk}(\mathbf{x} - \mathbf{y})F_k,$$

with the summation convention.
Flow due to a slender body with centreline $\mathbf{X}(s)$ can be expressed approximately as,

$$u_j(\mathbf{x}) = \int_0^L S_{jk}(\mathbf{x}, \mathbf{X}(s'))f_k(s')ds',$$

where the force per unit length $f_k(s')$ is determined so that $u_j(\mathbf{X}(s) + a\mathbf{n}(s)) \approx \partial_t \mathbf{X}(s)$ where $\mathbf{n}(s)$ is a vector normal to the centreline and a is slender body radius (small).
There are quite a few variants of slender body theory and associated error analyses developed in the 1970s (Lighthill, Batchelor, Cox, Johnson...). The above is accurate to $O(\sqrt{a})$ in theory and often works better in practice.

More modern methods

More modern approaches include the use of boundary integral methods (surface integrals of stokeslets), regularised stokeslets, hybrid regularised stokeslet-boundary element methods, force-coupling methods, finite elements...

More modern methods

More modern approaches include the use of boundary integral methods (surface integrals of stokeslets), regularised stokeslets, hybrid regularised stokeslet-boundary element methods, force-coupling methods, finite elements...
This talk will however work with a local approximation to slender body theory, and its generalisation to include viscoelastic effects.

Resistive force theory

Recall the relation $f_n = C_n u_n, f_t = C_t u_t$ with $C_n/C_t \approx 2$. This can be derived by neglecting the 'non-local' part of the integral,

$$u_j(\mathbf{X}(s)) = \int_{|s-s'|<q} S_{jk}(\mathbf{x}, \mathbf{X}(s')) f_k(s') ds' + \cancel{\int_{|s-s'|\geqslant q} S_{jk}(\mathbf{x}, \mathbf{X}(s')) f_k(s') ds'},$$

for a parameter $q = O(\sqrt{a})$.

Local coordinates: tangential component

Moving into a local coordinate system such that the section of flagellum for $s - q < s' < s + q$ is centred at the origin and lies along the x_1 axis, we can consider what force per unit length would be needed to produce velocity u_t in the x_1-direction and u_n in the x_2 (or x_3) direction at $x_1 = 0$, $x_2^2 + x_3^2 = a^2$:

Local coordinates: tangential component

Moving into a local coordinate system such that the section of flagellum for $s - q < s' < s + q$ is centred at the origin and lies along the x_1 axis, we can consider what force per unit length would be needed to produce velocity u_t in the x_1-direction and u_n in the x_2 (or x_3) direction at $x_1 = 0$, $x_2^2 + x_3^2 = a^2$:

$$u_t \approx \frac{1}{8\pi} \int_{-q}^{q} \left(\frac{1}{\sqrt{s^2 + a^2}} + \frac{(-s)^2}{(s^2 + a^2)^{3/2}} \right) f_t \, ds.$$

Local coordinates: tangential component

Moving into a local coordinate system such that the section of flagellum for $s - q < s' < s + q$ is centred at the origin and lies along the x_1 axis, we can consider what force per unit length would be needed to produce velocity u_t in the x_1-direction and u_n in the x_2 (or x_3) direction at $x_1 = 0$, $x_2^2 + x_3^2 = a^2$:

$$u_t \approx \frac{1}{8\pi} \int_{-q}^{q} \left(\frac{1}{\sqrt{s^2 + a^2}} + \frac{(-s)^2}{(s^2 + a^2)^{3/2}} \right) f_t \, ds.$$

Evaluating the integral and taking the leading order terms yields,

$$u_t \approx \frac{f_t}{8\pi} \left(4 \ln \left(\frac{2q}{a} \right) - 2 \right).$$

Local coordinates: normal component

Repeating this process for velocity u_n in the x_2 direction:

Local coordinates: normal component

Repeating this process for velocity u_n in the x_2 direction:

$$u_n \approx \frac{1}{8\pi} \int_{-q}^{q} \left(\frac{1}{\sqrt{s^2 + a^2}} + \frac{x_2^2}{(s^2 + a^2)^{3/2}} \right) f_n ds.$$

Notice we now have a term which varies azimuthally, x_2. This can be cancelled by adding a dipole distribution, or alternatively we can just take its azimuthal average, $< x_2^2 >=< a^2 \cos^2 \theta >= a^2/2$. Then,

$$u_n \approx \frac{f_n}{8\pi} \left(2 \ln \left(\frac{2q}{a} \right) + 1 \right).$$

Resitive force theory

The (Gray & Hancock 1955) resistive force coefficients are then,

$$C_t = \frac{4\pi}{2\ln\left(\frac{2q}{a}\right) - 1}, \quad C_n = \frac{8\pi}{2\ln\left(\frac{2q}{a}\right) + 1}.$$

Resitive force theory

The (Gray & Hancock 1955) resistive force coefficients are then,

$$C_t = \frac{4\pi}{2\ln\left(\frac{2q}{a}\right) - 1}, \quad C_n = \frac{8\pi}{2\ln\left(\frac{2q}{a}\right) + 1}.$$

The slender body integral equation can then be approximated as,

$$\begin{aligned} u_j(\mathbf{X}(s)) &\approx t_j C_t^{-1} \mathbf{t} \cdot \mathbf{f} + n_j C_n^{-1} \mathbf{n} \cdot \mathbf{f} \\ &= \mathbf{e}_j \cdot \mathsf{C}^{-1} \cdot \mathbf{f}, \end{aligned}$$

where $\mathsf{C}^{-1} = C_t^{-1}\mathbf{tt} + C_n^{-1}\mathbf{nn}$.

Weak viscoelastic effects: Linearised Maxwell fluid

Mucus is viscoelastic, indeed so is the analogue fluid (methylcellulose) we use in the lab: typical relaxation time 0.006 s (compared with 10–20 Hz beat frequency).

Weak viscoelastic effects: Linearised Maxwell fluid

Mucus is viscoelastic, indeed so is the analogue fluid (methylcellulose) we use in the lab: typical relaxation time 0.006 s (compared with 10–20 Hz beat frequency).
To estimate the effect of this, we considered a linearised version of the (dimensionless) Maxwell fluid model,

$$(1 + \lambda \partial_t)\, \tau_{jk} = (\partial_j u_k + \partial_k u_j),$$

Weak viscoelastic effects: Linearised Maxwell fluid

Mucus is viscoelastic, indeed so is the analogue fluid (methylcellulose) we use in the lab: typical relaxation time 0.006 s (compared with 10–20 Hz beat frequency).
To estimate the effect of this, we considered a linearised version of the (dimensionless) Maxwell fluid model,

$$(1 + \lambda\partial_t)\,\tau_{jk} = (\partial_j u_k + \partial_k u_j),$$

or

$$\tau_{jk} = \mathcal{L}(\partial_j u_k + \partial_k u_j).$$

Fundamental solution of Linearised Maxwell fluid (Smith, Gaffney & Blake)

The Maxwell-Stokes flow equations with forcing singular in time and space are,

$$-\boldsymbol{\nabla} p + \mathcal{L}\nabla^2 \mathbf{u} + \mathbf{e}_k \delta(\mathbf{x}, t) = 0.$$

Fundamental solution of Linearised Maxwell fluid (Smith, Gaffney & Blake)

The Maxwell-Stokes flow equations with forcing singular in time and space are,

$$-\boldsymbol{\nabla} p + \mathcal{L}\nabla^2 \mathbf{u} + \mathbf{e}_k \delta(\mathbf{x}, t) = 0.$$

We can then construct a solution $\tilde{P}_k, \tilde{S}_{jk}$ from the Newtonian Stokeslet,

$$\tilde{P}_k(\mathbf{x}, t) := P_k(\mathbf{x})\delta(t), \quad \tilde{S}_{jk}(\mathbf{x}, t) := S_{jk}(\mathbf{x})\left(1 + \lambda\partial_t\right)\delta(t).$$

Viscoelastic slender body theory

We will construct a solution through an integral both along arclength and in time (assuming zero flow for $t \leqslant 0$):

$$\begin{aligned}\mathbf{u}(\mathbf{x},t) &= \int_{0-}^{t+}\int_{0}^{L} \tilde{S}_{jk}(\mathbf{x}-\mathbf{X}(s'),t-t')f_k(\mathbf{s'},t')ds'dt', \\ &= \int_{0-}^{t+}\int_{0}^{L} (1+\lambda\partial_t)\,\delta(t-t')S_{jk}(\mathbf{x}-\mathbf{X}(s'))f_k(s',t')ds'dt',\end{aligned}$$

where $0-$ and $t+$ denotes limits taken from below at zero and from above at t.

Viscoelastic slender body theory

Let $T_1 < 0$ and $T_2 > t$, with $H(t)$ being a test function. Then,

$$\int_{T_1}^{T_2} (1 + \lambda \partial_t)\delta(t - t')H(t')dt' = H(t) + \lambda H'(t).$$

Viscoelastic slender body theory

Let $T_1 < 0$ and $T_2 > t$, with $H(t)$ being a test function. Then,

$$\int_{T_1}^{T_2} (1 + \lambda \partial_t)\delta(t - t')H(t')dt' = H(t) + \lambda H'(t).$$

Apply the above with,

$$H(t') := \int_0^L S_{jk}(\mathbf{x} - \mathbf{X}(s'))f_k(s', t')ds'$$

and take limits as $T_1 \uparrow 0$ and $T_2 \downarrow t$, to deduce that for $t > 0$,

Viscoelastic slender body theory

Let $T_1 < 0$ and $T_2 > t$, with $H(t)$ being a test function. Then,

$$\int_{T_1}^{T_2} (1 + \lambda \partial_t)\delta(t - t')H(t')dt' = H(t) + \lambda H'(t).$$

Apply the above with,

$$H(t') := \int_0^L S_{jk}(\mathbf{x} - \mathbf{X}(s'))f_k(s', t')ds'$$

and take limits as $T_1 \uparrow 0$ and $T_2 \downarrow t$, to deduce that for $t > 0$,

$$\mathbf{u}(\mathbf{x}, t) = (1 + \lambda \partial_{t'}) \int_0^L S_{jk}(\mathbf{x} - \mathbf{X}(s', t'))f_k(s', t')ds' \Big|_{t'=t}.$$

Maxwell resistive force theory

Applying the same local approximation as for the Newtonian case then yields (for planar motion),

$$u_n \approx C_n^{-1}(f_n + \lambda \partial_t f_n), \quad u_t \approx C_n^{-1}(f_t + \lambda \partial_t f_t).$$

Maxwell resistive force theory

Applying the same local approximation as for the Newtonian case then yields (for planar motion),

$$u_n \approx C_n^{-1}(f_n + \lambda \partial_t f_n), \quad u_t \approx C_n^{-1}(f_t + \lambda \partial_t f_t).$$

These relations provide a means to approximate the force per unit length on an imaged flagellum by solving a pair of ordinary differential equations.

Outline

Motivation

The above shows how the local force per unit length on the flagellum can be approximated from experimental data. One question of interest is, what does the internal active structure of the flagellum have to do in order to create this fluid dynamic force – and how much energy is required?

Motivation

The above shows how the local force per unit length on the flagellum can be approximated from experimental data. One question of interest is, what does the internal active structure of the flagellum have to do in order to create this fluid dynamic force – and how much energy is required?

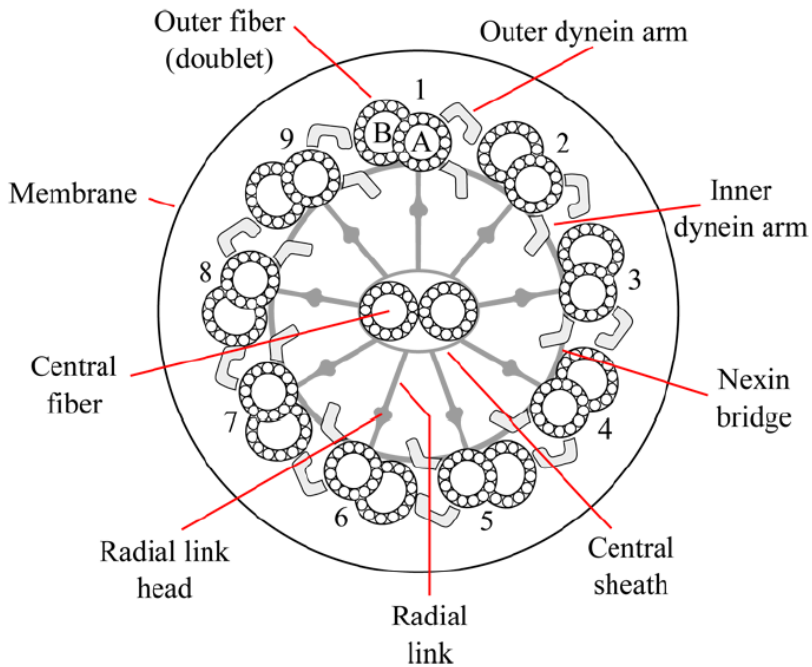

Bending and motion of cilia and flagella is produced as a result of relative sliding of adjacent microtubule doublets, produced by the motor protein, dynein ATPase.

Dynamics of an elastic rod with external forcing

- Consider a one-dimensional curved rod $\mathbf{X}(s)$ bending in a plane, with tangent angle $\phi(s)$ relative to a fixed axis.

Dynamics of an elastic rod with external forcing

- Consider a one-dimensional curved rod $\mathbf{X}(s)$ bending in a plane, with tangent angle $\phi(s)$ relative to a fixed axis.
- Considering the rod as two segments $[0, s]$ and $(s, L]$, we can define the contact moment $M(s)$ and contact force $\mathbf{F}(s)$ exerted by the distal segment $[s, L]$ on the proximal segment $[0, s]$ at $\mathbf{X}(s)$.

Dynamics of an elastic rod with external forcing

- Consider a one-dimensional curved rod $\mathbf{X}(s)$ bending in a plane, with tangent angle $\phi(s)$ relative to a fixed axis.
- Considering the rod as two segments $[0, s]$ and $(s, L]$, we can define the contact moment $M(s)$ and contact force $\mathbf{F}(s)$ exerted by the distal segment $[s, L]$ on the proximal segment $[0, s]$ at $\mathbf{X}(s)$.
- At the distal end, $\mathbf{N}(L) = 0$ and $M(L) = 0$.

Dynamics of an elastic rod with external forcing

Taking a small strain, finite curvature (ϕ_s) constitutive model for elasticity:

$$M(s) = E(s)\phi_s(s).$$

Dynamics of an elastic rod with external forcing

Taking a small strain, finite curvature (ϕ_s) constitutive model for elasticity:

$$M(s) = E(s)\phi_s(s).$$

The surrounding fluid exerts a force per unit length $\mathbf{f}(s)$. Force balance and the distal boundary condition yield,

$$\mathbf{N}(s) = \int_s^L \mathbf{f}\, ds'.$$

Dynamics of an elastic rod with external forcing

Taking a small strain, finite curvature (ϕ_s) constitutive model for elasticity:

$$M(s) = E(s)\phi_s(s).$$

The surrounding fluid exerts a force per unit length $\mathbf{f}(s)$. Force balance and the distal boundary condition yield,

$$\mathbf{N}(s) = \int_s^L \mathbf{f}\, ds'.$$

Moment balance on an infinitesimal segment of the rod then yields,

$$\mathbf{n} \cdot \int_s^L \mathbf{f}\, ds' + \partial_s(E\kappa) = 0,$$

where $\mathbf{n}$ is a unit normal.

Flagellar bending stiffness $E(s)$

Based on micrograph data on thinning of the sperm flagellum we can approximate $E(s)$ by a quadratic,

$$E_b(s) = \begin{cases} (E_p - E_d)\left(\frac{s-s_d}{s_d}\right)^2 + E_d & s \leqslant s_d \\ E_d & s > s_d. \end{cases}$$

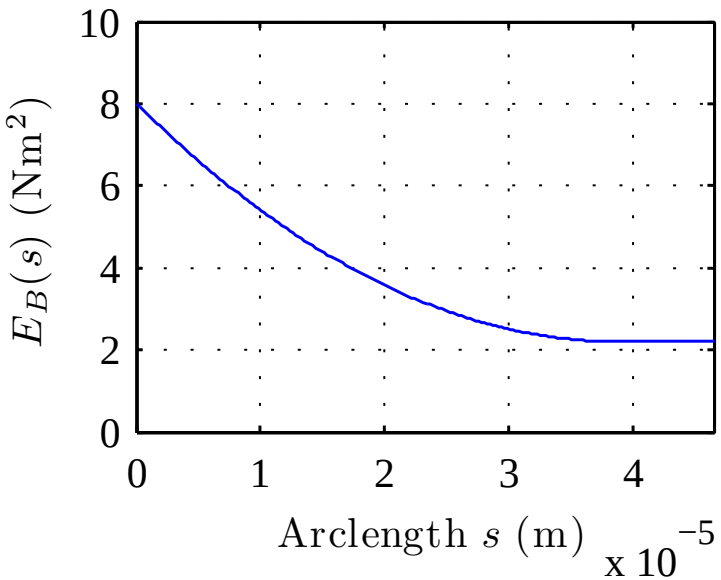

Active moments

The simplest model of an active flagellum decomposes it into a compound structure of two effective 'filaments' separated by distance b, with interfilament force per unit length having tangential component $f(s)$ (so that the moment per unit length is bf).

Active moments

The simplest model of an active flagellum decomposes it into a compound structure of two effective 'filaments' separated by distance b, with interfilament force per unit length having tangential component $f(s)$ (so that the moment per unit length is bf).

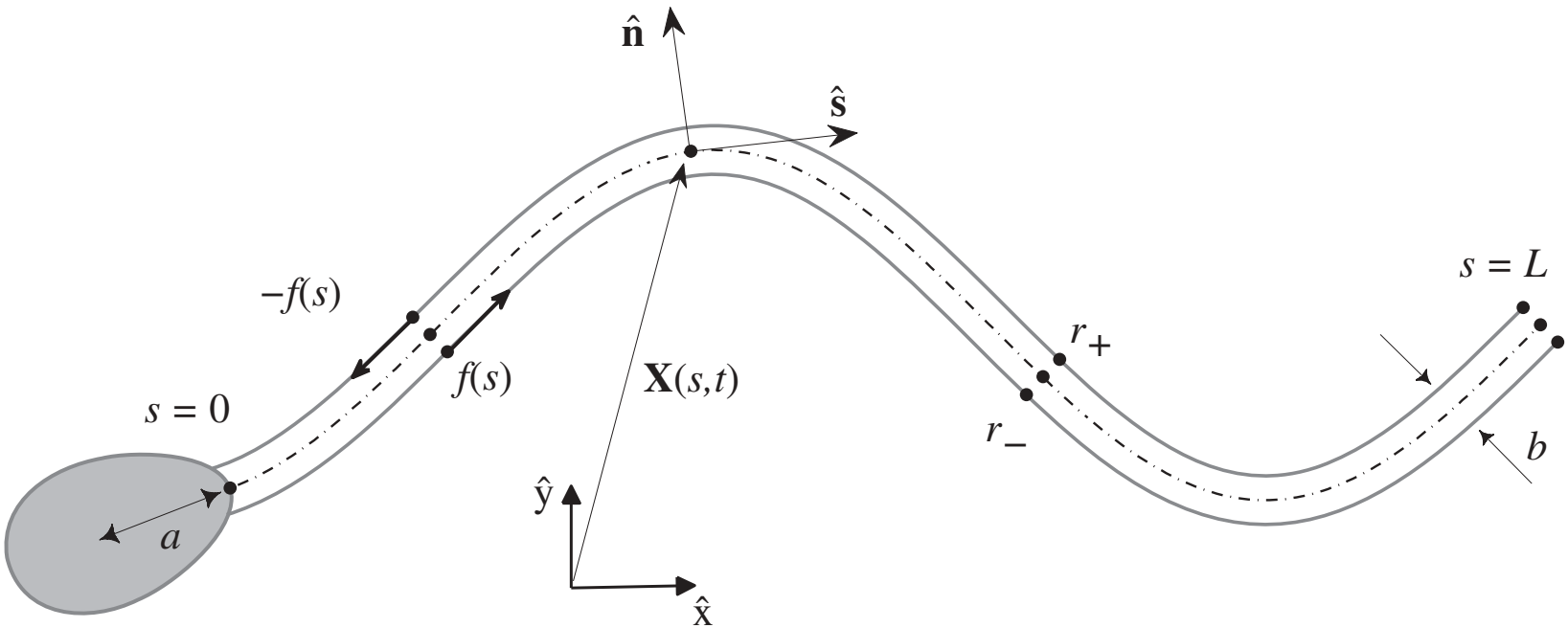

Sliding filament elastohydrodynamics

Modelling each filament as an elastic rod with tangential interfilament force f, leads to the elastohydrodynamic equation,

$$\mathbf{n} \cdot \int_s^L \mathbf{f} ds' + bf + \partial_s(E\kappa) = 0.$$

Sliding filament elastohydrodynamics

Modelling each filament as an elastic rod with tangential interfilament force f, leads to the elastohydrodynamic equation,

$$\mathbf{n} \cdot \int_s^L \mathbf{f} ds' + bf + \partial_s(E\kappa) = 0.$$

The interfilament force f arises from both active motor proteins (dynein ATPase) and passive elastic bonds (nexin links, radial spokes):

$$f = f^d + f^p.$$

Sliding filament elastohydrodynamics

Modelling each filament as an elastic rod with tangential interfilament force f, leads to the elastohydrodynamic equation,

$$\mathbf{n} \cdot \int_s^L \mathbf{f} ds' + bf + \partial_s(E\kappa) = 0.$$

The interfilament force f arises from both active motor proteins (dynein ATPase) and passive elastic bonds (nexin links, radial spokes):

$$f = f^d + f^p.$$

Introduce the relative sliding between the filaments, $\Delta(s)$. A linear elastic passive resistance $f^p = -K\Delta$.

Basal sliding

For small separation between the filaments we have the approximate relation,

$$\Delta(s) = \Delta(0) + b(\phi(s) - \phi(0)).$$

If the filaments are restrained at the base so that $\Delta(0) =: \Delta_0 = 0$ then we have simply,

$$\Delta(s) = b(\phi(s) - \phi(0)).$$

Basal sliding

For small separation between the filaments we have the approximate relation,

$$\Delta(s) = \Delta(0) + b(\phi(s) - \phi(0)).$$

If the filaments are restrained at the base so that $\Delta(0) =: \Delta_0 = 0$ then we have simply,

$$\Delta(s) = b(\phi(s) - \phi(0)).$$

If however (as is probable) relative sliding does occur, then we need to model the basal compliance. Taking a linear model with stiffness ξ and balancing the jump in contact force at the base yields,

$$\int_0^L f ds' = \xi \Delta_0.$$

Basal sliding

Integrating the elastohydrodynamic equation and rearranging then yields,

$$\Delta_0 = \frac{1}{\xi b}\left(-\int_0^L \mathbf{n}(s)\cdot\int_s^L \mathbf{f}(s')ds'ds + E\phi_s(0)\right).$$

Basal sliding

Integrating the elastohydrodynamic equation and rearranging then yields,

$$\Delta_0 = \frac{1}{\xi b}\left(-\int_0^L \mathbf{n}(s)\cdot\int_s^L \mathbf{f}(s')ds'ds + E\phi_s(0)\right).$$

After some further rearranging we can then estimate the internal active force per unit length f^d from the fluid dynamic force per unit length $\mathbf{f}$:

$$\begin{aligned} f^d = &-\frac{\mathbf{n}(s)}{b}\cdot\int_s^L \mathbf{f}\,ds' - \frac{1}{b}\partial_s(E\phi_s) + bK(\phi-\phi_0) \\ &+ \frac{K}{\xi b}\left(-\int_0^L \mathbf{n}(s)\cdot\int_s^L \mathbf{f}(s')ds'ds + E\phi_s(0)\right). \end{aligned}$$

Parameterisation and results

There is uncertainty regarding basal stiffness ξ, however f^d more closely resembles a travelling wave for $\xi \geqslant 0.1$ N/m (significantly stiffer than say sea urchin). We should be able to recover this through micromanipulation and 'counterbend' observation in human cells.

Parameterisation and results

By examining micromanipulation data on animal sperm and making appropriate scalings we can estimate most of the parameters for the human sperm model.

E_p ($\times 10^{-21}$ Nm^2)	E_d ($\times 10^{-21}$ Nm^2)	K_p ($\times 10^3$ N/m^2)	K_d ($\times 10^3$ N/m^2)	ξ (N/m)
8	2.2	2	2	**0.1**

Parameterisation and results

By examining micromanipulation data on animal sperm and making appropriate scalings we can estimate most of the parameters for the human sperm model.

E_p ($\times 10^{-21}$ Nm^2)	E_d ($\times 10^{-21}$ Nm^2)	K_p ($\times 10^{3}$ N/m^2)	K_d ($\times 10^{3}$ N/m^2)	ξ (N/m)
8	2.2	2	2	**0.1**

$\Delta(s,t)$ (m)

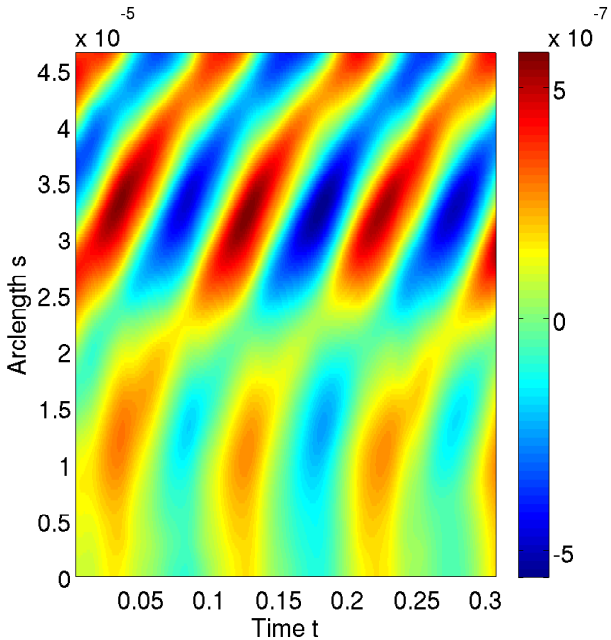

$f^d(s,t)$ (N/m)

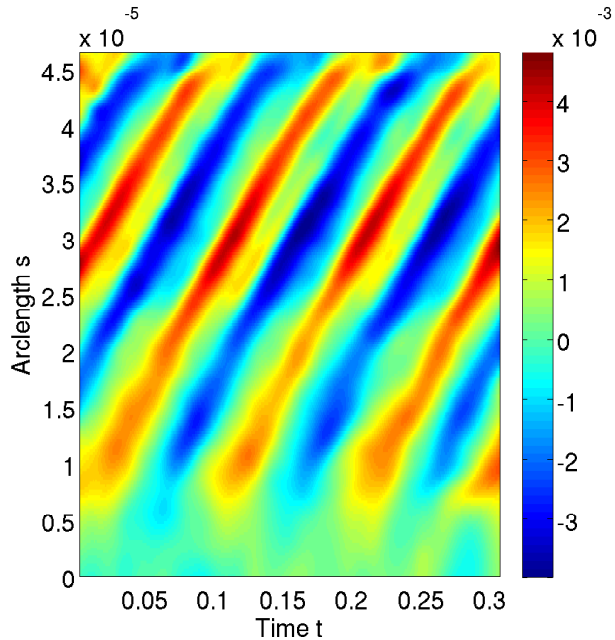

Parameterisation and results

By examining micromanipulation data on animal sperm and making appropriate scalings we can estimate most of the parameters for the human sperm model.

E_p ($\times 10^{-21}$ Nm^2)	E_d ($\times 10^{-21}$ Nm^2)	K_p ($\times 10^{3}$ N/m^2)	K_d ($\times 10^{3}$ N/m^2)	ξ (N/m)
8	2.2	2	2	**0.1**

$\Delta(s,t)$ (m)

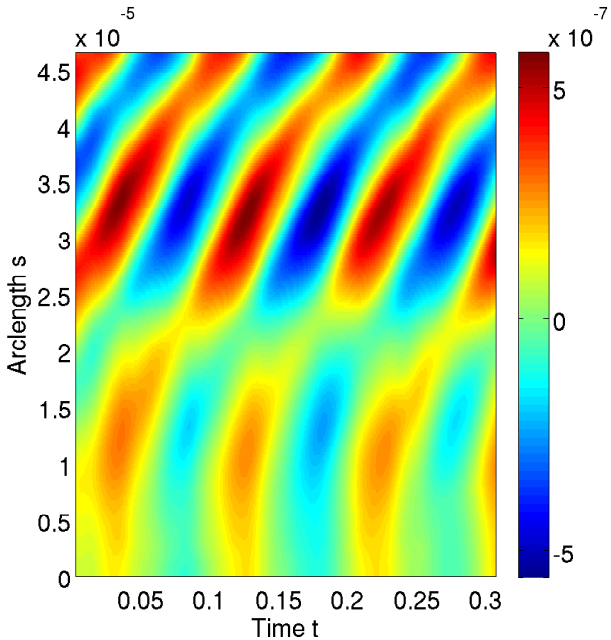

$f^d(s,t)$ (N/m)

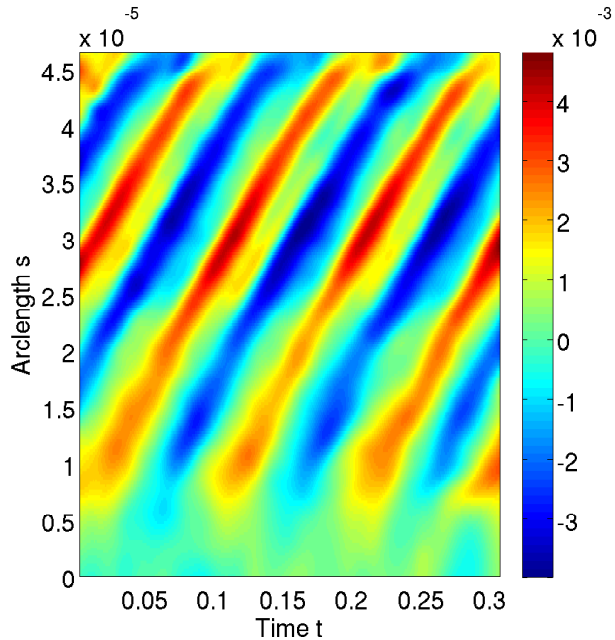

A peak active force density of 5×10^{-3} N/m [=5 pN/nm] is consistent with data on dynein density and peak force.

Complex compliance model

We can use this method to assess the 'complex compliance' model of dynein activity of F. Jülicher and colleagues, $\hat{\Delta} = k\hat{f}^d$ for some parameter $k \in \mathbb{C}$ by taking a discrete Fourier transform.

$$|\hat{\Delta}| = |k||\hat{f}^d|, \quad \arg\hat{\Delta} = \arg\hat{f}^d + \arg k.$$

Complex compliance model

We can use this method to assess the 'complex compliance' model of dynein activity of F. Jülicher and colleagues, $\hat{\Delta} = k\hat{f}^d$ for some parameter $k \in \mathbb{C}$ by taking a discrete Fourier transform.

$$|\hat{\Delta}| = |k||\hat{f}^d|, \quad \arg\hat{\Delta} = \arg\hat{f}^d + \arg k.$$

Modulus

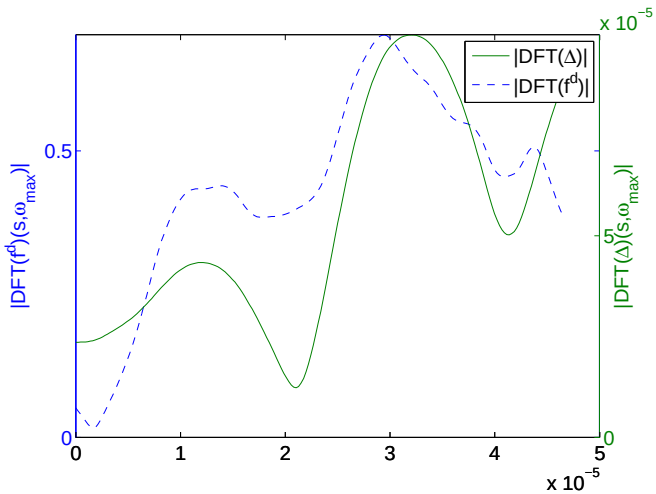

Argument

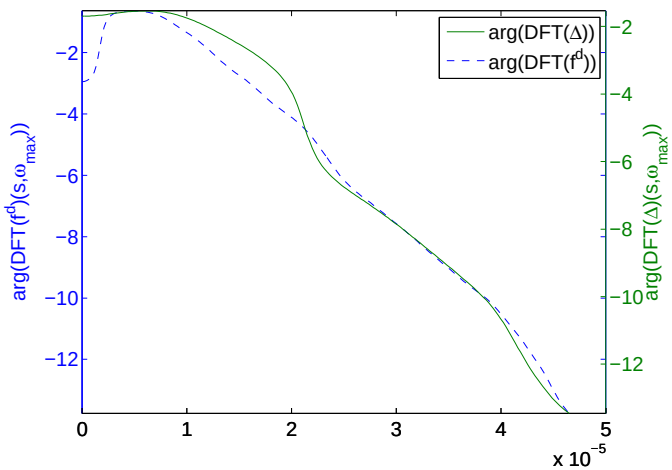

Rate of working

Material points of the upper and lower filaments are given by,

$$\mathbf{X}^{\pm}(s,t) := \mathbf{X}(s,t) \pm (b\mathbf{n}(s,t) + \Delta(s,t)\mathbf{t}(s,t)).$$

Rate of working

Material points of the upper and lower filaments are given by,

$$\mathbf{X}^{\pm}(s,t) := \mathbf{X}(s,t) \pm (b\mathbf{n}(s,t) + \Delta(s,t)\mathbf{t}(s,t)).$$

Calculating $\partial_t \mathbf{X}^{\pm}(s,t)$ and multiplying by the force components $\pm f(s,t)\mathbf{t}(s,t)$ yields the rate of working as simply,

$$f\Delta_t = (f^d + f^p)\Delta_t.$$

Rate of working

Material points of the upper and lower filaments are given by,

$$\mathbf{X}^{\pm}(s,t) := \mathbf{X}(s,t) \pm (b\mathbf{n}(s,t) + \Delta(s,t)\mathbf{t}(s,t)).$$

Calculating $\partial_t \mathbf{X}^{\pm}(s,t)$ and multiplying by the force components $\pm f(s,t)\mathbf{t}(s,t)$ yields the rate of working as simply,

$$f\Delta_t = (f^d + f^p)\Delta_t.$$

The rate of working of the active elements is then,

$$\Delta_t f^d = \Delta_t(K\Delta + f) = {}^1\!/_2 K\partial_t\Delta^2 + (\Delta_{0t} + b\phi_t - b\phi_{0t})f.$$

Biochemical energy

- Chemical energy (ATP/ADP ratio) is generated by the mitochondria (at the base of the flagellum) and diffuses / is transported along the flagellum.

Biochemical energy

- Chemical energy (ATP/ADP ratio) is generated by the mitochondria (at the base of the flagellum) and diffuses / is transported along the flagellum.
- There may also exist glycolytic enzymes running the length of the flagellum: the relative importance (particularly in high viscosity migration) is disputed.

Biochemical energy

- Chemical energy (ATP/ADP ratio) is generated by the mitochondria (at the base of the flagellum) and diffuses / is transported along the flagellum.
- There may also exist glycolytic enzymes running the length of the flagellum: the relative importance (particularly in high viscosity migration) is disputed.
- It is possible to suppress different metabolic pathways, e.g. with cyanide and to observe the effects on swimming behaviour.

Biochemical energy

- Chemical energy (ATP/ADP ratio) is generated by the mitochondria (at the base of the flagellum) and diffuses / is transported along the flagellum.
- There may also exist glycolytic enzymes running the length of the flagellum: the relative importance (particularly in high viscosity migration) is disputed.
- It is possible to suppress different metabolic pathways, e.g. with cyanide and to observe the effects on swimming behaviour.
- Energetic mechanisms are also a possible target for fertility-promoting drugs and contraceptives. α-chlorohydrin (blocks sperm-specific GAPDH in glycolysis) was nearly such a contraceptive.

Distal rate of working

One interesting quantity is how much power needs to be supplied to the distal segment $[s, L]$ averaged over time,

$$< W(s) >= \frac{1}{T} \int_0^T \int_s^L \Delta_t f^d ds' dt.$$

Distal rate of working

One interesting quantity is how much power needs to be supplied to the distal segment $[s, L]$ averaged over time,

$$< W(s) >= \frac{1}{T} \int_0^T \int_s^L \Delta_t f^d ds' dt.$$

After some more manipulation, one can derive,

$$\begin{aligned} W(s) &= \int_s^L \Delta_t f^d ds' \\ &= \frac{1}{2}\partial_t \int_s^L K\Delta^2 ds' + \frac{1}{2}\partial_t \int_s^L E\phi_s^2 ds' + \partial_t \mathbf{X} \cdot \int_s^L \mathbf{f} ds' \\ &+ (\Delta_t - b\phi_t) \int_s^L f ds' - \phi_t E\phi_s(L) + \phi_t E\phi_s - \int_s^L \partial_t \mathbf{X} \cdot \mathbf{f} ds'. \end{aligned}$$

Distal rate of working

One interesting quantity is how much power needs to be supplied to the distal segment $[s, L]$ averaged over time,

$$< W(s) >= \frac{1}{T} \int_0^T \int_s^L \Delta_t f^d ds' dt.$$

After some more manipulation, one can derive,

$$\begin{aligned} W(s) &= \int_s^L \Delta_t f^d ds' \\ &= \frac{1}{2}\partial_t \int_s^L K\Delta^2 ds' + \frac{1}{2}\partial_t \int_s^L E\phi_s^2 ds' + \partial_t \mathbf{X} \cdot \int_s^L \mathbf{f} ds' \\ &+ (\Delta_t - b\phi_t) \int_s^L f ds' - \phi_t E\phi_s(L) + \phi_t E\phi_s - \int_s^L \partial_t \mathbf{X} \cdot \mathbf{f} ds'. \end{aligned}$$

The first two terms average to zero.

Distal rate of working

One interesting quantity is how much power needs to be supplied to the distal segment $[s, L]$ averaged over time,

$$< W(s) >= \frac{1}{T} \int_0^T \int_s^L \Delta_t f^d ds' dt.$$

After some more manipulation, one can derive,

$$\begin{aligned} W(s) &= \int_s^L \Delta_t f^d ds' \\ &= \frac{1}{2}\partial_t \int_s^L K\Delta^2 ds' + \frac{1}{2}\partial_t \int_s^L E\phi_s^2 ds' + \partial_t \mathbf{X} \cdot \int_s^L \mathbf{f} ds' \\ &+ (\Delta_t - b\phi_t) \int_s^L f ds' - \phi_t E\phi_s(L) + \phi_t E\phi_s - \int_s^L \partial_t \mathbf{X} \cdot \mathbf{f} ds'. \end{aligned}$$

The first two terms average to zero. The mean rate of working $< W(s) >$ is therefore given by the time-averages of the remaining terms, which quantify rate of working by contact force, contact force jump, contact moment and viscous dissipation.

Notation

$$
\begin{aligned}
W^d &= \int_s^L \Delta_t f^d ds', \\
W^f &= \int_s^L \Delta_t f ds', \\
W^{mp} &= \phi_t E \phi_s, \\
W^c &= (\partial_t \mathbf{X}) \cdot \int_s^L \mathbf{f} ds', \\
W^j &= (\Delta_t - b\phi_t) \int_s^L \mathbf{f} ds'
\end{aligned}
$$

Rate of working

(a) W^d

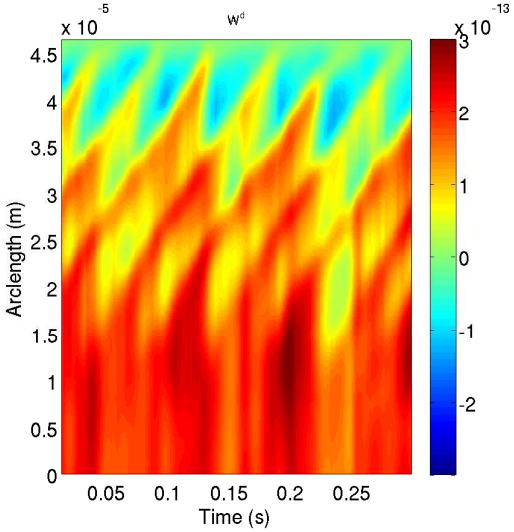

(b) $\langle W^d \rangle$, $\langle W^f \rangle$

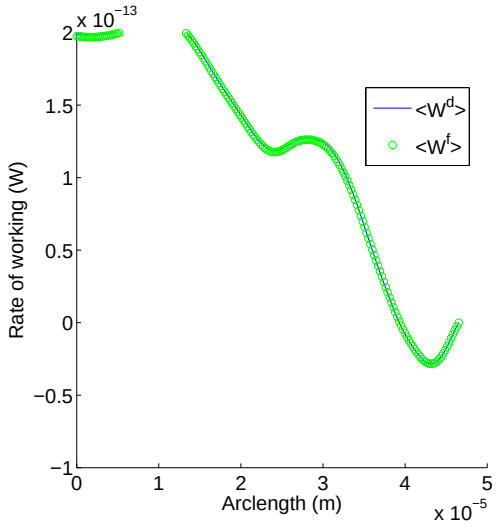

(c) W^{mp}

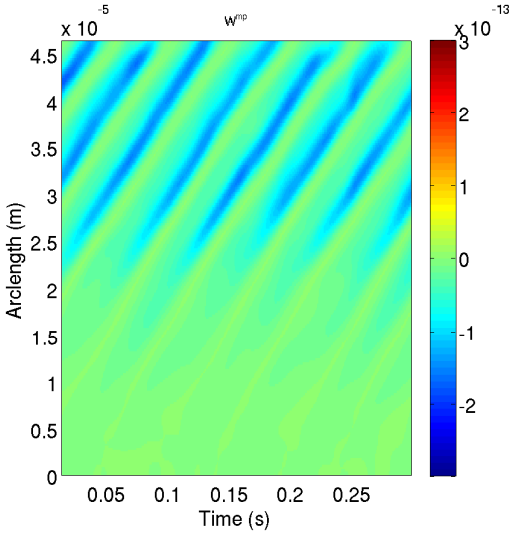

(d) $\langle W^c \rangle$, $\langle W^{mp} \rangle$, $\langle W^j \rangle$

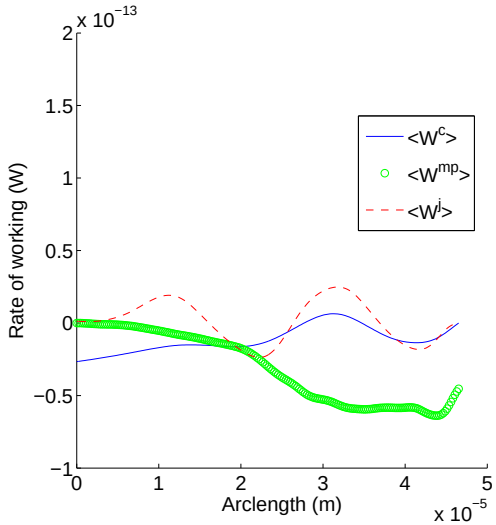

Observations

- The rate of working in the distal flagellum is not as large as might be naively expected from looking at the flagellum shape.

Observations

- The rate of working in the distal flagellum is not as large as might be naively expected from looking at the flagellum shape.
- This effect is produced by energy transport by the contact moment, i.e. transport of elastic bending energy.

Observations

- The rate of working in the distal flagellum is not as large as might be naively expected from looking at the flagellum shape.
- This effect is produced by energy transport by the contact moment, i.e. transport of elastic bending energy.
- So we can partially 'rescue' the idea (dating back to the 1950s) that elastic waves are important in transporting energy.

Observations

- The rate of working in the distal flagellum is not as large as might be naively expected from looking at the flagellum shape.
- This effect is produced by energy transport by the contact moment, i.e. transport of elastic bending energy.
- So we can partially 'rescue' the idea (dating back to the 1950s) that elastic waves are important in transporting energy.
- Further experimental work is needed to refine the parameterisation. However this method may be useful in interpreting pharmacological experiments.

Acknowledgements

- Funding: MRC, Birmingham Science City
- Colleagues: Hermes Gadêlha, Eamonn Gaffney, John Blake, Jackson Kirkman-Brown, Birmingham Women's Hospital.